Nuclear Materials and Energy 19 (2019) 211–217

Contents lists available at ScienceDirect

Nuclear Materials and Energy

journal homepage: www.elsevier.com/locate/nme

EDGE2D-EIRENE predictions of molecular emission in DIII-D high-recycling divertor plasmas

M. Groth[a,*], E.M. Hollmann[b], A.E. Jaervinen[c], A.W. Leonard[d], A.G. McLean[c], C.M. Samuell[c], D. Reiter[e], S.L. Allen[c], P. Boerner[e], S. Brezinsek[e], I. Bykov[b], G. Corrigan[f], M.E. Fenstermacher[c], D. Harting[f], C.J. Lasnier[c], B. Lomanowski[a], M.A. Makowski[c], M.W. Shafer[g], H.Q. Wang[h], J.G. Watkins[i], S. Wiesen[e], R.S. Wilcox[g], the DIII-D team[1]

[a] Aalto University, Espoo, Finland
[b] University of California San Diego, San Diego, CA, USA
[c] Lawrence Livermore National Laboratory, Livermore, CA, USA
[d] General Atomics, San Diego, CA, USA
[e] Forschungszentrum Jülich GmbH, Institute for Energy and Climate Research Plasma Physics, Jülich, Germany
[f] Culham Centre for Fusion Energy, Culham Science Centre, Abingdon, UK
[g] Oak Ridge National Laboratory, Oak Ridge, TN, USA
[h] Oak Ridge Associated Universities, Oak Ridge, TN, USA
[i] Sandia National Laboratory, Albuquerque, NM, USA

ARTICLE INFO

Keywords:
Deuterium atomic and molecular emission
Lyman-Werner and Fulcher band
DIII-D
Divertor edge fluid simulations
EDGE2D-EIRENE
EIRENE

ABSTRACT

The contributions of deuterium molecular emission to the total deuterium radiation was assessed in DIII-D ohmically-confined plasmas in high-recycling divertor conditions. Radial profiles of the deuterium Ly-α line intensity across the low-field side divertor leg were obtained with the recently installed divertor Survey Poor Resolution, Extended Spectrometer [1]. A high-resolution spectrometer was used to measure the poloidal profiles of the deuterium Balmer-α and the deuterium Fulcher-α band intensity in the visible wavelength range. The scrape-off layer plasma and neutral distributions were simulated using the edge fluid EDGE2D-EIRENE [2], and the numerical solutions constrained utilizing Thomson scattering and Langmuir probe measurements at the low-field side midplane and the divertor target plate. The studies show that for these conditions molecular emission plays a negligible role in the total radiative power balance of the low-field side divertor, but molecular processes are important when evaluating deuterium Balmer-α line intensity for code-experiment validation.

1. Introduction

Radiation from neutral and charged species in the scrape-off layer (SOL) in fusion devices dissipates plasma energy and thus plays a critical role reducing the power fluxes to plasma-facing components [3]. In diverted tokamaks, the strongest line emission from hydrogen atoms and low-charge state impurities are observed in the divertor at plasma (electron) temperatures (T_e) below 5 eV and 30 eV for hydrogen and impurity radiation, respectively (carbon-based PFC: [4,5], metal-based PFC: [6]). In detached divertor conditions of low temperature ($T \lesssim 1$ eV) and high (electron, atom, and molecular) density ($n > 1 \times 10^{20}$ m^{-3}), radiation from excited molecules may be strong enough to impact the radiative power balance in the divertor. Spectroscopic measurements and collisional-radiative simulations of an inductively-coupled laboratory hydrogen plasma showed that emission from the Lyman-Werner bands (900–1500 Å) could exceed atomic hydrogen emission dominated by Lyman-alpha (Ly-α, 1215.7 Å) [7]. Since the fuel ions are preferentially recycled as molecules in devices with carbon-based plasma-facing components [8], such as the DIII-D tokamak, the molecular contribution to the total radiation may be accentuated in these devices. To explore and characterize the contributions from molecular emission, experiments were carried out in DIII-D in a lower single-null configuration utilizing the comprehensive suite of lower divertor diagnostics, including a new divertor Survey, Poor Resolution, Extended spectrometer (DivSPRED, [1]), the Multi-chord Divertor Spectrometer (MDS) [9] and the Divertor Thomson Scattering

* Corresponding author.
E-mail address: mathias.groth@aalto.fi (M. Groth).
[1] See Appendix of W.M. Solomon et al., "DIII-D research advancing the scientific basis for burning plasmas and fusion energy", Nucl. Fusion **57** (2017) 102018.

https://doi.org/10.1016/j.nme.2019.02.035
Received 10 August 2018; Received in revised form 13 February 2019; Accepted 24 February 2019

(DTS) system [10]. The obtained plasmas were simulated with the edge fluid code EDGE2D [11], iteratively coupled to the neutral Monte-Carlo code EIRENE [12], and further interpreted with standalone EIRENE runs including additional synthetic diagnostics. The primary purpose of these studies is to determine the significance of molecular emission in cold and dense divertor conditions, and to clarify whether it provides an additional plasma channel explaining the previously observed mismatch between measured and predicted divertor emission and plasma conditions [13,14].

2. Experimental analyses of divertor conditions and radiation in high-recycling conditions

Low-recycling, high-recycling and partially detached divertor plasma conditions at the low-field side (LFS) divertor target were established by varying the core plasma density through deuterium injection into the DIII-D main chamber. In this publication, deuterium-only, ohmic plasmas of approximately 0.9–1.1 MW heating power, supplemented with 10-ms short in 100-ms periods neutral beam blips for charge-exchange ion-temperature measurements are analyzed. The initial preference of ohmic over higher-power, thus higher-density, high-confinement mode (H-mode) discharges is primarily driven by the higher quality of the experimental data in the former confinement regime. Whether and how much the impact of molecular radiation is in higher-density H-mode plasmas is deferred to future publications. The plasma current was 1.1 MA, the toroidal field 2.1 T, with the ion **B**x∇B drift direction into the lower divertor. The plasma-facing components in DIII-D are ATJ graphite; hence, carbon is the primary plasma impurity species (of approximately concentration 1% just inboard of the separatrix at the LFS midplane) in DIII-D. Radial and poloidal profiles of the divertor plasma conditions and radiation were obtained by radially sweeping the divertor X-point / strike points across the diagnostics lines-of-sight. In these experiments, the high-field side (HFS) strike point remained on the divertor floor, including the 45-degree target plate, throughout the sweep, while the LFS strike point was swept across the lower divertor extended baffle (shelf), as in ref. [15].

DTS measurements of the electron temperature (T_e), made directly adjacent to the LFS target plate, approximately 5 mm above the target plate, show the expected decrease of peak T_e ($T_{e,pk,LFS\text{-}plate}$) from 25 – 30 eV in low-recycling conditions, to 2–3 eV in high-recycling conditions and $\lesssim$ 1 eV in partially detached conditions (Fig. 1a). Simultaneously, the peak electron density ($n_{e,pk,LFS\text{-}plate}$) increased from 10^{19} m^{-3} to 2–3 × 10^{20} m^{-3} and 4 × 10^{20} m^{-3} (Fig. 1b). In these studies, the electron density at the separatrix on LFS midplane, $n_{e,sep,LFS\text{-}mp}$, was determined via the electron temperature at the same location, $T_{e,sep,LFS\text{-}mp}$, which was approximated by an extended two-point model relationship given in ref. [16]. Langmuir probe measurements at the LFS target plate [17] show that the peak ion saturation current, $j_{sat,pk,LFS\text{-}plate}$, saturated at the intermediate to high values of $n_{e,sep,LFS\text{-}mp}$, and only decreased significantly, at the highest $n_{e,sep,LFS\text{-}mp}$ indicating partial detachment (Fig. 1c). (The issue of how steep or even bifurcated the reduction in $j_{sat,pk,LFS\text{-}plate}$ is with respect to $n_{e,sep,LFS\text{-}mp}$ strongly depends on the assumed value of $n_{e,sep,LFS\text{-}mp}$. Its discussion is beyond of the scope of this paper.)

Despite raising the gain of the DivSPRED system to its maximum, and saturating the prominent Ly-α (and CIII and CIV) lines, the Lyman and Werner bands were not resolved with the present DivSPRED in high-recycling conditions (Fig. 2a, wavelength resolution approximately 1 Å/pixel). Hence, for these studies, Lyman-Werner band intensities, and thus the energy emitted in these bands, are assumed to be at least two orders of magnitude lower than Ly-α photons. Similar to Hollmann et al. [20], emission from the D_2 Fulcher-α band was measured in four identical discharges to cover the triplet Q-branch for

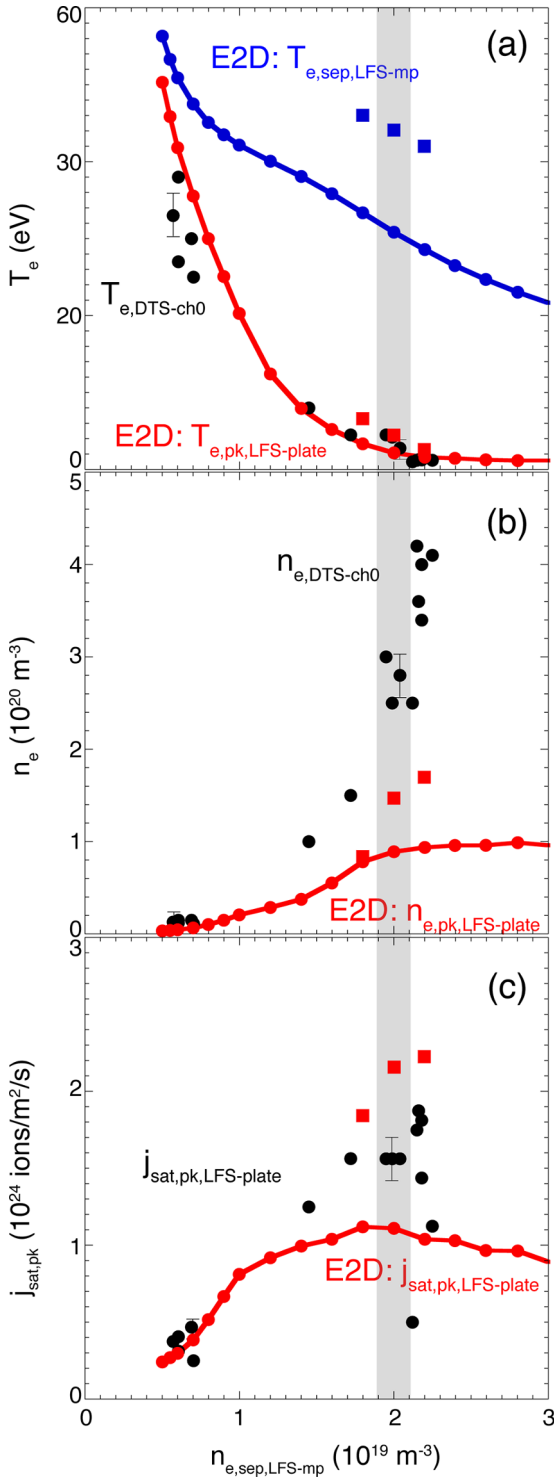

Fig. 1. Peak electron temperature ($T_{e,DTS\text{-}ch0}$, a) and density ($n_{e,DTS\text{-}ch0}$, b) measured at the lowest DTS channel (approximately 5 mm vertically off the LFS plate), and the peak ion saturation current ($j_{sat,pk,LFS\text{-}plate}$, c) as a function of the electron density at the separatrix at the LFS midplane ($n_{e,sep,LFS\text{-}mp}$). The measured values are given by the black circles, the EDGE2D-EIRENE predictions at $P_{core\text{-}bd}$ = 0.9 MW by the red, connected circles, the predictions at $P_{core\text{-}bd}$ = 1.4 MW by the red, unconnected squares. The EDGE2D-EIRENE predicted electron temperature at the LFS midplane ($T_{e,sep,LFS\text{-}mp}$) in (a) is given by the blue, connected circles for $P_{core\text{-}bd}$ = 0.9 MW, and by the blue unconnected squares for $P_{core\text{-}bd}$ = 1.4 MW. The EDGE2D-EIRENE catalogue names are listed in Appendix A.

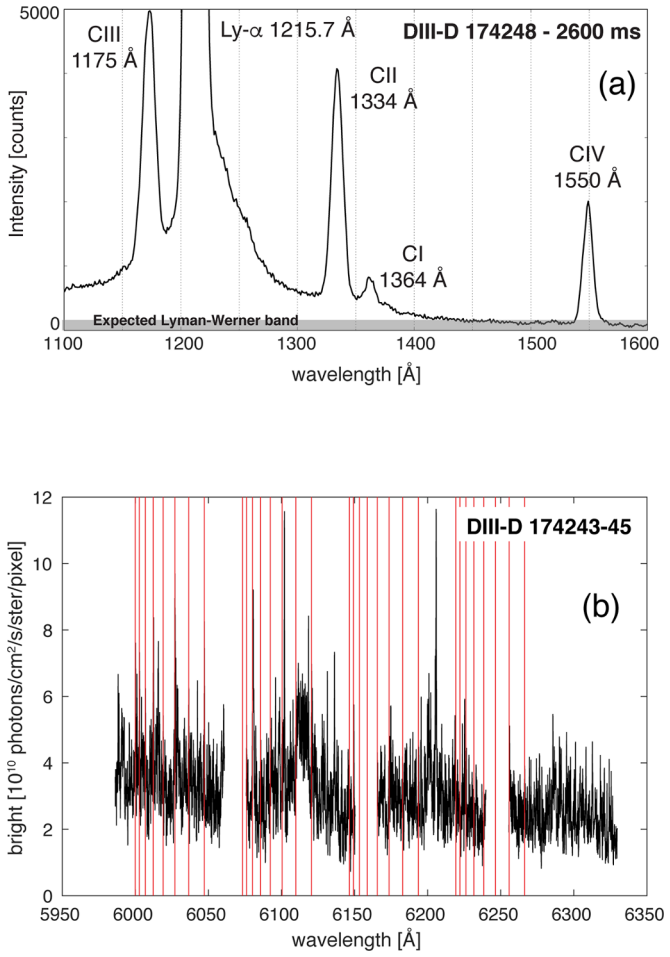

Fig. 2. Spectra of the deuterium and carbon emission in the EUV (a, DIII-D 174248) and the Fulcher-α band in the visible wavelength ranges (b, DIII-D 174243–45) for DIII-D high-recycling conditions. The anticipated Lyman-Werner bands in the EUV spectrum is indicated by the horizontal grey bar. The Fulcher-α spectrum is a composite spectrum of four identical discharges covering the Q-branch up to a vibrational quantum number 4 within the wavelength range 5980 Å to 6330 Å. The vertical red lines denote the assumed first four vibrational Fulcher bands, v′ = v″ = 0, 1, 2 and 3, which have been fitted with a different rotational temperature for each vibrational level.

vibrational quantum states of up to 4 (v′ = v″ = 0, 1, 2, 3, 4) across the wavelength range 5980 to 6330 Å (Fig. 2b, wavelength resolution approximately 0.1 Å/pixel).

In high-recycling conditions at the LFS divertor plate the measured poloidal profile of the deuterium Ly-α and the Balmer-α (D_α, 6561 Å) line intensities across the divertor floor peaked at the common flux side of the HFS and LFS strike point regions (Fig. 3a and b). While the absolute calibration of the DivSPRED with visible line ratios is in progress, the measured peak Ly-α line intensity is scaled up to the EDGE2D-EIRENE predicted peak Ly-a line intensity in Fig. 3a. Including the HFS target region, the peak D_α intensity is approximately four times higher at the HFS than at the LFS strike zone (Fig. 4) consistent with the cross-field drift-driven deuteron flow pattern observed in DIII-D [18] and other tokamaks (see e.g., [19]). Lastly, the measured radial profile plate of the D_2 Fulcher-α band intensity across the LFS divertor plate, inferred from measuring the triplet Q-branch for vibrational quantum states of 4 (v′ = v″ = 0, 1, 2, 3, 4, see ref. [20]), also peaks at the common flux region adjacent to the strike (Fig. 3c). Here, the total Fulcher band intensity is the inferred Q-branch intensity multiplied by a factor of 2 to account for the corresponding P branch. Outside the uncertainties of the spectroscopic measurements, the Fulcher-α band intensity peaks 2–3 cm radially outward of the peaks in Ly-α and D_α;

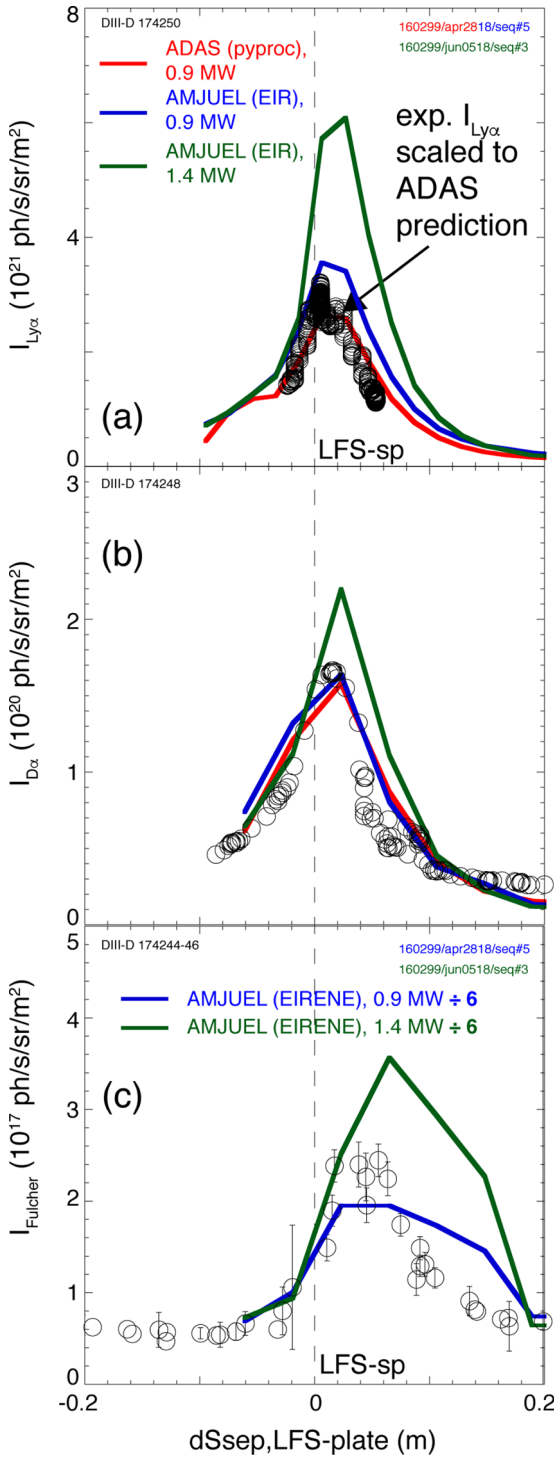

Fig. 3. Radial profiles of the Ly-α (a), D_α (b) and Fulcher-α band (c) intensities across the LFS plate as function of distance from the LFS strike point. The measurements are given by the black open circles, the ADAS predictions at $P_{core\text{-}bd}$ = 0.9 MW by the red line, and the AMJUEL predictions at $P_{core\text{-}bd}$ = 0.9 MW and 1.4 MW by the blue and green lines, respectively. The AMJUEL predicted Fulcher-α band intensities were scaled down by a factor of 6 to be approximately at the same peak intensity as the measurements. The corresponding DIII-D discharge numbers and EDGE2D-EIRENE catalogue names are given in the figure labels. The dashed vertical line indicates the radial position of the separatrix at the LFS plate.

the radial profile of the Fulcher-α band intensity has the same width as radial profile of the D_α intensity. The peak intensity of the total Fulcher-α band is almost three orders of magnitude lower than the peak D_α line

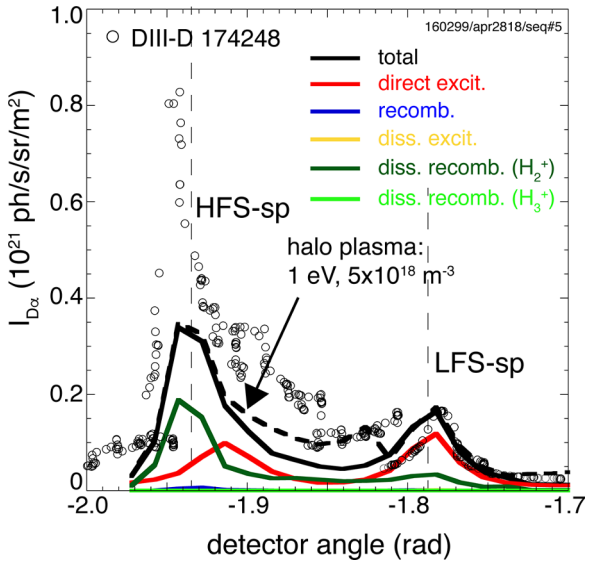

Fig. 4. Poloidal profiles, including the HFS and LFS target regions, of the measured (DIII-D 174248) and EIRENE (AMJUEL) predicted radiative components to the D_α line intensity due to atomic and molecular processes: red - direct excitation, blue – 3-body recombination, yellow - dissociative excitation, dark green - dissociative recombination from H_2^+, light green - dissociative recombination from H_3^+. The total D_α line intensity (solid black) assuming a vacuum halo region is compared to a case assuming, ad-hoc, $T_e = 1$ eV and $n_e = 5x10^{18}/m^3$ for the halo region. The corresponding EDGE2D-EIRENE catalogue name is given in the figure. The dashed vertical lines indicate the radial position of the separatrix at the HFS and LFS plates.

intensity. Given the close proximity of the Fulcher-α band and D_α wavelengths, the power radiated by Fulcher-α photons is thus also three orders of magnitudes lower than the power in D_α photons and hence insignificant compared to the energy of Ly-α photons.

3. Setup of EDGE2D-EIRENE and EIRENE simulations

The EDGE2D-EIRENE code package [2] with boundary conditions and radial transport model closely adapted to the experiment was used to predict the SOL plasma and neutral particle conditions in the LFS divertor leg. The fluid edge code EDGE2D [11] solves the Bragiinski fluid equations in the parallel-**B** direction and assumes a diffusive-convective model in the radial direction. Here, diffusive transport expressed through transport coefficients for particles ($D_\perp$), and for the ion and electron energies (χ_i and χ_e, respectively) was invoked. Cross-field drifts due to **ExB** and **B**x∇B for deuterons and carbon ions were included in the simulations. In these studies, to match the measured radial profiles of n_e at the LFS midplane, a transport barrier across the separatrix was imposed by reducing $D_\perp$ from 0.5 m^2/s to 0.25 m^2/s inside the separatrix, corresponding to the n_e pedestal region, and then raised exponentially to 4.5 m^2/s to obtain the measured fall-off of the n_e across the SOL (approximately 5 cm). Similarly, to reproduce the measured T_e profile at the LFS midplane, χ_e was raised from 1 m^2/s in the core region to 2 m^2/s in the SOL, while a constant χ_i of 0.75 m^2/s in both the core and SOL regions were assumed. Below the X-point, spatially constant diffusivities (initially, $D_\perp = \chi_e = 1$ m^2/s, $\chi_i = 0.75$ m^2/s) were assumed. Furthermore, a total heating power of 0.9 MW across the EDGE2D core boundary, $P_{core\text{-}bd}$, split equally between ions and electrons, was assumed in the simulations presented here, which is consistent with the total heating power and bolometry measurements inside the separatrix.

The neutral Monte-Carlo code EIRENE [12] solves the kinetic Boltzmann equations for atomic and molecular hydrogen species in plasmas, and it is iteratively coupled to EDGE2D to provide the particle, momentum and energy sources and sinks to the plasma code. The (coupled) EDGE2D-EIRENE calculations were carried out on a non-orthogonal grid including the SOL and the pedestal region. EIRENE utilizes the EDGE2D grid, but also extends to the actual main chamber and PFR walls (halo plasma region); for the EDGE2D-EIRENE runs vacuum was assumed for the halo plasma region. The impact of assuming a low-T_e (0.5 – 2 eV), low-n_e (1×10^{18}–1×10^{19} m^{-3}) halo plasma region on the deuterium intensities was assessed in separate, standalone EIRENE runs. In these simulations the updated atomic and molecular densities, fluxes and radiation losses were not yet fed back into the EDGE2D-EIRENE plasma solver. Hence, the plasma solution did not change due to the introduction of the halo plasma. Atomic and molecular rates were taken from the AMJUEL database [21], and the currently most complete EIRENE model [22] was used to account for hydrogen ion-molecular interaction at high divertor densities ($> 10^{20}$ m^{-3}). Recovering the previous capability of EIRENE to predict the total Fulcher band intensity [8,23] AMJUEL was also updated with the equivalent reduced population coefficients for the Lyman and Werner bands using molecular data provided by Sawada and Fujimoto [21,24]. Post-processing of the deuterium line intensities was carried out using the ADAS [25] database in EDGE2D-EIRENE and AMJUEL in standalone EIRENE along identical lines of sight. Opacity of Ly-α photons in EIRENE is not considered in these analyses as the module is not yet available at the writing of this report.

Consistent with the experimental setup, in the simulations deuterium was injected from the outermost grid boundary at the top of the plasma and pumped below the divertor shelf by imposing an albedo (of value 0.94) on a user-specified surface on the EIRENE grid. (The actual sub-divertor geometry was not yet included.) The walls and targets are assumed fully saturated and thus non-pumping surfaces, which is likely to be an over-simplification and to be assessed in future studies. Deuterons were fully recycled at the divertor targets and the outermost EDGE2D grid cells as either atoms or molecules, using the TRIM database [26] for deuterium particle and energy reflections on carbon. Carbon was sputtered as atoms at the targets by both deuterium ions and atoms, and by atoms only at the main chamber and private flux region wall, using the Haasz-Davis sputtering yield from 1997 [27]. (Other yield databases were also tested and will be published separately.) Release of carbon as hydrocarbon molecules was omitted in these studies. Upon ionization, carbon is simulated as a fluid species, following a momentum balance equation in the parallel-**B** direction [28], and diffusion in the radial-**B** direction. Here, a spatially constant $D_\perp$ of 1 m^2/s was applied to entire simulation grid due to the lack of measured radial profiles of the carbon densities (both total and for individual charge states).

4. EDGE2D-EIRENE predictions of plasma and neutral conditions at LFS plate

Qualitatively consistent with our expectations and the experiments, raising $n_{e,sep,LFS\text{-}mp}$ through D_2 injection at constant power across the EDGE2D core boundary ($P_{core\text{-}bd}$) and assuming identical transport coefficients, lowers both $T_{e,sep,LFS\text{-}mp}$ and $T_{e,pk,LFS\text{-}plate}$ (Fig. 1a), and increases both $n_{e,pk,LFS\text{-}plate}$ and $j_{sat,pk,LFS\text{-}plate}$ (Fig. 1b and 1c, respectively). While EDGE2D-EIRENE predicts the LFS plate condition in low-recycling conditions, $n_{e,sep,LFS\text{-}mp} \approx 6$–$8 \times 10^{18}$ m^{-3}, well within the uncertainty of the DTS measurements, in high-recycling conditions, $n_{e,sep,LFS\text{-}mp} \approx 1.8$–$2.2 \times 10^{19}$ m^{-3}, $T_{e,sep,LFS\text{-}mp}$ decreased below 30 eV, which is inconsistent with previous measurements using a reciprocating Langmuir probe [13]. Furthermore, the simulations under-predict $n_{e,pk,LFS\text{-}plate}$ by a factor of 2–3, and $j_{sat,pk,LFS\text{-}plate}$ by a factor of 2, including the saturation of $j_{sat,pk,LFS\text{-}plate}$ with $n_{e,sep,LFS\text{-}mp}$ only. To recover $T_{e,sep,LFS\text{-}mp}$ above 30 eV as implied by an extended two-point model postulated in ref. [16], in these studies $P_{core\text{-}bd}$ was raised ad-hoc from 0.9 MW to 1.4 MW. The increase in power raised $T_{e,pk,LFS\text{-}plate}$ from 2 eV to 4 eV, and $j_{sat,pk,LFS\text{-}plate}$ from 1×10^{24} ions/m^2/s to 2×10^{24} ions/m^2/s, which is (still) consistent with the DTS and the target Langmuir

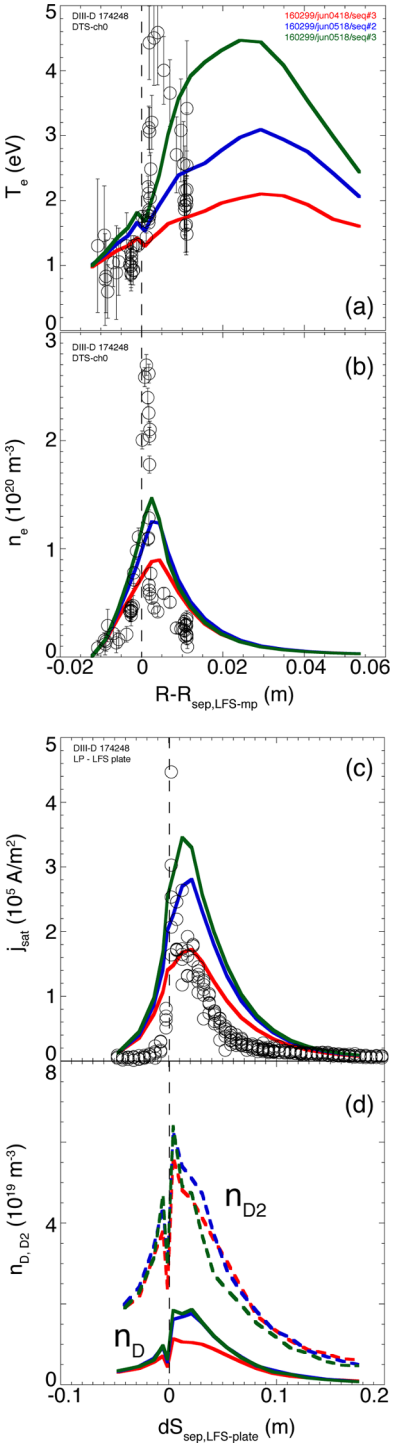

Fig. 5. Radial profiles of the electron temperature (T_e, a) and density (n_e, b) measured at the lowest DTS channel across the LFS plate as a function of distance from the separatrix referenced to the LFS midplane (R-$R_{sep,LFS-mp}$). (c) Radial profiles of the ion saturation current (j_{sat}) measured by Langmuir probes embedded in the LFS target as a function of distance from the separatrix at the LFS target. (d) EDGE2D-EIRENE predicted molecular (dashed lines) and atomic (solid lines) densities as a function of distance from the separatrix at the LFS target. The measurements are given by the black open circles, and the EDGE2D-EIRENE predictions at $n_{e,sep,LFS-mp}$ = 2.0x10^{19}/m^3 and $P_{core-bd}$ = 0.9 MW, 1.2 MW and 1.4 MW by the red, blue and green lines, respectively. The dashed vertical line indicates the radial position of the separatrix in the LFS divertor / at the LFS plate.

probe measurements. However, $n_{e,pk,LFS-plate}$ remained a factor of 2 lower than measured.

For high-recycling conditions, EDGE2D-EIRENE predicts $T_{e,pk,LFS-plate}$ of 4 eV when assuming $P_{core-bd}$ = 1.4 MW (green curve) instead of 0.9 MW (red) and 1.1 MW (blue), which are more consistent with the experiments, but indicate approximately 5x broader T_e profiles than observed experimentally (Fig. 5a). These observations were found to be robust against reductions of χ_e and χ_i from 1.0 m^2/s to 0.2 m^2/s in the divertor, and the removal of the transport barrier above the X-point (predictions not shown in Fig. 5). The predicted T_e and n_e profiles agree both in absolute value and radial fall-off with the DTS measurements at the LFS X-point (data not shown). At the LFS plate, however, the predicted n_e (Fig. 5b) and j_{sat} profiles (Fig. 5c) are significantly narrower than the T_e profiles. The predicted n_e and j_{sat} profiles were found to be insensitive to lowering $D_\perp$ and $\chi_{e,i}$ below the X-point from 1 m^2/s to 0.2 m^2/s (predictions not shown in Fig. 5), and cannot be explained by variations in the absolute value of $n_{e,sep,LFS-mp}$. Further comparison to the DTS measurements indicates that the broadening of the predicted radial profiles of T_e and n_e occurs within 5 cm off the target plate, hence, below the ionization front. Assuming constant radial diffusivities in the model may thus be insufficient to capture the underlying physics. Within the present parameter scans for high-recycling SOL conditions, the strongest response of the LFS divertor conditions was found to be on $P_{core-bd}$: $n_{e,pk,LFS-plate}$ and $j_{sat,pk,LFS-plate}$ increase by 50% when raising $P_{core-bd}$ from 0.9 MW to 1.4 MW.

For high-recycling conditions, the EIRENE predicted molecular density (n_{D2}) directly adjacent to the LFS plate is 2–3 higher than the atomic density (n_D) indicating that the deuterons are predominantly recycled as molecules off the carbon surfaces (Fig. 5d, as expected and consistent with previous studies [20]). Spatially, both n_{D2} and n_D peak in the common flux region directly adjacent to the separatrix, and n_{D2} is of the same order of magnitude as n_e. n_{D2} was found to be nearly invariant against raising $P_{core-bd}$ from 0.9 MW to 1.4 MW, while n_D increased by 50% due to higher heating power.

5. ADAS and AMJUEL predictions of atomic and molecular deuterium emission

Utilizing the plasma conditions at the LFS plate predicted by EDGE2D-EIRENE for the high-recycling conditions described in section IV, both the ADAS and AMJUEL predicted D_α profiles are quantitatively consistent with the measured profiles at the LFS plate (Fig. 3b). Using EIRENE and its native AMJUEL data, the peak D_α line intensity is identical to the D_α line intensity predicted by EDGE2D-EIRENE using ADAS. It is worth noting that while the ADAS and AMJUEL predictions are identical for high-recycling conditions at the LFS plate, molecular processes, and in particular the contribution of dissociative recombination significantly raises the EIRENE predicted D_α line intensity by a factor of 3 across the detached HFS (Fig. 4). Three-body volume recombination and dissociative excitation of D_2 are predicted not to play a role in the divertor plasmas investigated here (Fig. 4). These EIRENE predictions are inconsistent with previous work by the (same) authors [20], and could not be resolved by the time of writing of this paper. Secondly, while raising $P_{core-bd}$ from 0.9 MW to 1.4 MW has a negligible effect on the EIRENE predicted D_α intensity across the LFS divertor (Fig. 3b), it does raise the predicted D_α intensity by 50% across the HFS divertor due to the stronger non-linearity of the emission rate coefficients in the range of 1 to 2 eV (HFS) versus 2 to 4 eV (LFS). (Fig. 4). It is important to call attention to the fact that the predicted D_α intensity across the HFS divertor is still 2.5 times lower than measured.

Similarly, both the EGDE2D-EIRENE and standalone EIRENE predicted Ly-α line intensities across the LFS divertor leg respond to the change of the atomic and molecular model and of $P_{core-bd}$ as does the D_α intensity (Fig. 3a). For purpose of illustration only, pending post-

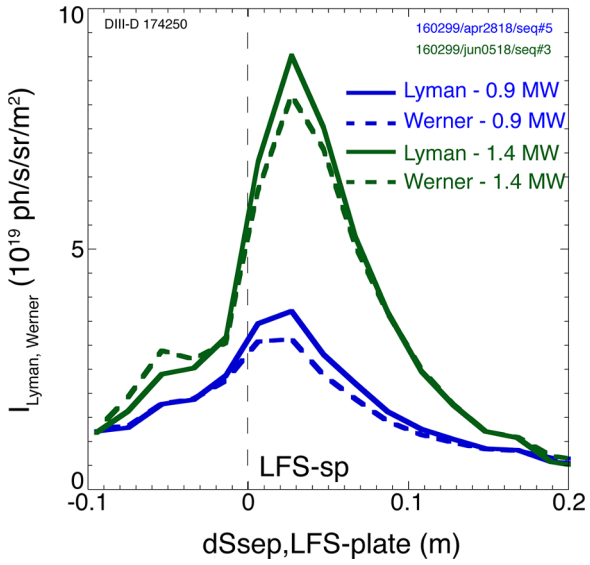

Fig. 6. Radial profiles of the EIRENE (AMJUEL) predicted intensities of the Lyman (solid lines) and Werner bands (dashed lines) across the LFS plate as a function of radial distance from the LFS strike point. The predictions assuming $P_{core\text{-}bd}$ = 0.9 MW and 1.4 MW are given the blue and green lines, respectively. The corresponding EDGE2D-EIRENE catalogue names are given in the figure labels. The dashed vertical line indicates the radial position of the separatrix at the LFS plate.

calibration, the measured peak intensity of Ly-α was scaled to the ADAS predicted value. It is worth noting that, unlike the D_α line intensity, the EIRENE predicted Ly-α line intensity across the LFS divertor leg is predominately driven by direct excitation. Other processes, such as dissociative recombination from D_2^+ and D_3^+, as well as the dissociative excitation of D_2, are taken into account, but are predicted not play a significant role. Hence, for Ly-α line intensity, these simulations indicate an approximately 20% discrepancy between ADAS and AMJUEL for high-recycling conditions potentially due to differences in the rate coefficients in the atomic databases.

The EIRENE predicted peak Fulcher-α band intensity, using AMJUEL data, over-predicts the measured peak Fulcher-α band intensity by a factor of 5 (Fig. 3c). Here, the AMJUEL predicted Fulcher-α band intensities were scaled down by a factor of 6 to be approximately at the same peak intensity as the measurements. The predicted profiles are approximately a factor of two broader than the measured ones, reflecting the broader than measured n_e and j_{sat} profiles at the LFS plate predicted by EDGE2D-EIRENE. Given the fact that EIRENE reproduced the D_α intensity well within the uncertainty of the measurements, the predictions of the Fulcher-α band suggest that the molecular density is significantly overestimated in the simulations.

Lastly, EIRENE predictions of the Lyman and Werner bands for the high-recycling conditions obtained at the LFS plate indicate that the total molecular emission is negligible compared to atomic emission from the Lyman series. The total predicted Lyman-Werner band intensity (Fig. 6) is a factor of 50 smaller than the predicted Ly-α intensity (Fig. 3a). Raising $P_{core\text{-}bd}$ from 0.9 MW to 1.4 MW, and thus T_e across the LFS plate, raised both the Lyman and Werner band intensities by about a factor of 3 to 4. Compared to the total radiated power in the simulations, shared approximately equally between deuterium and carbon radiation, the predicted molecular radiation is more than a factor 100 smaller than atomic deuterium, and carbon atomic and ionic line radiation.

6. Summary

Measurements and simulations using the EDGE2D-EIRENE and, in post-processing mode, standalone EIRENE codes show that for DIII-D ohmic plasmas in the high-recycling regime, D_2 emission play a negligible role in the radiative power balance of the divertor plasma in ohmic confinement. The measured EUV spectrum is dominated by Ly-α and several carbon ion lines [1], the molecular Lyman-Werner bands were too weak to be observed and to be resolved with the present DivSPRED system. In addition, the measured Fulcher-α band is approximately three orders of magnitude lower than the D_α intensity, further corroborating the negligible role molecular radiation plays in the radiative power balance in these high-recycling conditions. Correspondingly, the EIRENE predicted Lyman and Werner band radiation are approximately a factor of 50, and the Fulcher-α intensity two orders of magnitude lower than the predicted Ly-α and D_α intensities, respectively. The EIRENE studies indicate, however, that molecular processes, such as dissociative recombination, contribute up to 30% to the production of D_a line intensity in high-recycling divertor conditions, but more than 50% in detached conditions. The EIRENE predictions rely, however, critically on the EGDE2D-EIRENE predicted background plasma. While for high-recycling conditions the measured peak T_e of 3–4 eV in front of the LFS divertor plate were predicted by EDGE2D-EIRENE, the predicted T_e profiles are significantly (5x) broader than measured. Furthermore, the electron density in front of the plate was under-predicted by factors 2–3. These predictions were observed invariant against changes to the assumed radial transport, in these studies varied by a factor of 4, and responded to a 50% increase in the power across the EDGE2D-EIRENE core surface only, which is inconsistent with the experiment. Future studies will focus on further identifying the root causes for the discrepancy in the T_e and n_e profiles across the LFS divertor, and on utilizing the DTS measurements directly in EIRENE for the assessment of molecular versus atomic deuterium radiation. Furthermore, the EIRENE reflection and thermal release model will be revisited and the impact of deuterium fueling due to hydrocarbon release be assessed. While this publication focused on ohmic conditions, because of the superior data quality in this confinement regime, both the experimental data and numerical analyses presented here will be expanded to higher-power, higher-density H-mode plasmas in future studies.

Acknowledgements

This work was supported by US DOE under contract nos. DE-FC02-04ER54698, DE-AC52-07NA27344, and DE-FG92-07ER54917. The DIII-D data shown in this paper can be obtained in digital format by following the links at https://fusion.gat.com/global/D3D_DMP.

Disclaimer

This work has been carried out within the framework of the EUROfusion Consortium and has received funding from the Euratom research and training programme 2014–2018 under grant agreement number 633053. The views and opinions expressed herein do not necessarily reflect those of the European Commission.

Supplementary materials

Supplementary material associated with this article can be found, in the online version, at doi:10.1016/j.nme.2019.02.035.

Appendix A

Table A1

Table A1
List of EDGE2D-EIRENE catalogue names as stored on the JET Linux cluster freia (as of July 31, 2018).

$n_{e,sep,LFS\text{-}mp}$ [10^{19} m^{-3}]	$P_{core\text{-}bd}$ = 0.9 MW	$P_{core\text{-}bd}$ = 1.4 MW
0.5	mgroth/160299/may2118/2	
0.55	mgroth/160299/may2118/1	
0.6	mgroth/160299/may0318/1	
0.7	mgroth/160299/apr2318/1	
0.8	mgroth/160299/apr2318/2	
0.9	mgroth/160299/apr2318/3	
1.0	mgroth/160299/apr2318/4	
1.2	mgroth/160299/apr2518/4	
1.4	mgroth/160299/apr2518/5	
1.6	mgroth/160,99/apr2618/1	
1.8	mgroth/160299/apr2618/2	mgroth/160299/jun0618/3
2.0	mgroth/160299/apr2818/5	mgroth/160299/jun0518/3
2.2	mgroth/160299/apr2818/6	mgroth/160299/jul1218/1
2.4	mgroth/160299/may0118/2	
2.6	mgroth/160299/may0518/1	
2.8	mgroth/160299/may0218/2	
3.0	mgroth/160299/apr2818/4	

References

[1] A.G. Mclean, this conference.
[2] S. Wiesen, EDGE2D-EIRENE code interface report, JET ITC-Report, 2006, http://www.eirene.de/e2deir_report_30jun06.pdf.
[3] A. Loarte, et al., Nucl. Fusion 47 (2007) S203.
[4] R.C. Isler, et al., Phys. Plasmas 4 (1997) 355.
[5] C.F. Maggi, et al., J. Nucl. Mater. 241-243 (1997) 414.
[6] K.D. Lawson, et al., J. Nucl. Mater. 463 (2015) 463.
[7] U. Fantz, et al., Plasma Sources Sci. Technol. 25 (2016) 045006, , https://doi.org/10.1088/0963-0252/25/4/045006.
[8] S. Brezinsek, et al., J. Nucl. Mater. 313-316 (2003) 967.
[9] N.H. Brooks, et al., Rev. Sci. Instrum. 63 (1992) 5167.
[10] F. Glass, et al., Rev. Sci. Instrum. 87 (2016) 11E508.
[11] R. Simonini, et al., Contr. Plasma Phys. 34 (1994) 368.
[12] D. Reiter, et al., J. Nucl. Mater. 196-198 (1992) 80.
[13] M. Groth, et al., J. Nucl. Mater. 415 (2011) 056116.
[14] J.D. Canik, et al., Phys. Plasmas 24 (2017) 056116.
[15] A.G. McLean, et al., J. Nucl. Mater. 463 (2015) 533.
[16] A.W. Leonard, et al., Nucl. Fusion 57 (2017) 086033.
[17] J.G. Watkins, et al., Rev. Sci. Instrum. 79 (2008) 10F125.
[18] G.D. Porter, et al., Phys. Plasmas 7 (2000) 3663.
[19] S. Krashenninikov, et al., Phys. Plasmas 23 (2016) 055602.
[20] E.M. Hollmann, et al., Plasma Phys. Contr. Fusion 48 (2006) 1165.
[21] K. Sawada, et al., J. Appl. Phys. 78 (1997) 37.
[22] V. Kotov, et al., Plasma Phys. Contr. Fusion 50 (2008) 105012.
[23] U. Fantz, J. Nucl. Mater. 290-293 (2001) 367.
[24] Reiter et al., Forschungzentrum Juelich, Germany - http://eirene.de.
[25] H.P. Summers, et al., Plasma Phys. Contr. Fusion 48 (2006) 263.
[26] W. Eckstein, Computer Simulations of Ion-Solid Interaction, Springer, Berlin, 1991.
[27] J.W. Davis, et al., J. Nucl. Mater. 241-243 (1997) 37.
[28] J. Neuhauser, et al., Nucl. Fusion 24 (1984) 39.